PHOTONICS Research

High performance visible generation of Ho^{3+}-doped all-fiber lasers

Shuaihao Ji, Xuexian Lin, Bo Xiao, Zhongyu Wang, Xiuji Lin, and Zhiping Cai*

Department of Electronic Engineering, School of Electronic Science and Engineering (National Model Microelectronics College), Xiamen University, Xiamen 361005, China
**Corresponding author: zpcai@xmu.edu.cn*

Received 10 July 2023; revised 3 October 2023; accepted 7 October 2023; posted 11 October 2023 (Doc. ID 500147); published 24 November 2023

Direct generation of visible frequency from a compact all-fiber laser while preserving high output characteristics has been a subject of research in laser technology. We investigated the high output performance of all-fiber lasers based on Ho^{3+}-doped ZBLAN fluoride glass fiber especially operating in the deep-red band by pumping at 640 nm. Remarkably, we achieved a maximum continuous-wave output power of 271 mW at 750 nm with a slope efficiency of 45.1%, which represents, to our knowledge, the highest direct output power recorded in an all-fiber laser with a core diameter of less than 10 μm in the deep-red band. Additionally, we successfully developed a 1.2 μm all-fiber laser pumped by a 640 nm laser. We extensively investigated the correlation between these two-laser generation processes and their performances at 750 nm and 1.2 μm wavelengths. By increasing the pumping rate, we observed an efficient recycling of population through a highly excited state absorption process, which effectively returned the population to the upper laser level of the deep-red transition. Moreover, we determined the optimized conditions for such lasers, identified the processes responsible for populating the excited state energy levels, and established the corresponding spectroscopic parameters.

https://doi.org/10.1364/PRJ.500147

1. INTRODUCTION

All-fiber lasers are extensively utilized due to their compact structure, superior heat dissipation, and avoidance of the need for optical cavity cleaning, and these have various applications such as precision machining measurement, bio-photonics, and defense applications [1–4]. High power fiber lasers in the infrared optical region especially at 1, 1.53, and 2 μm are well studied with doped silicate glass fiber [5–9]. These lasers have achieved optical powers surpassing the kilowatt level. Besides, visible lasers have broken through the watt-level laser outputs [10–13]. However, the output power of the single cladding all-fiber laser in the visible band remains limited to 100 mW [14,15]. This can be mainly attributed to two primary factors. First, the fluoride fiber, which serves as the host for visible laser generation, has a low damage threshold [16]. Second, achieving high performance visible all-fiber laser mirrors has proven to be challenging [17].

In recent years, significant advancements have been made in the development of ultrafast visible lasers using various conventional methods to improve the visible mode-locking, such as Pr/Yb co-doped with a figure-eight cavity [18] and free space nonlinear polarization rotation in Dy^{3+}-, Ho^{3+}-, and Pr/Yb-doped fiber lasers [19–21]. However, the output power of all-fiber mode-locked lasers remains limited to a few milliwatts, restricting their applications. Therefore, it is important to continue exploring high performance all-fiber visible lasers, as achieving continuous wave output of visible light in an all-fiber structure serves as the foundation for harnessing high energy pulses.

Ho^{3+}-doped ZBLAN fluoride glass (ZFG) fibers have gained considerable attention due to their wide spectrum resources in the visible to near-infrared region [10,14,15,22–25]. These fibers provide three main pumping options for the visible light generation process. Blue laser diode (LD) pumping yields highly efficient green laser output albeit with limited beam quality. On the other hand, all-fiber deep-red lasers have a maximum output power of only 16 mW due to the long energy level lifetime of $^5I_7$. Red pumping covers a broader range of energy levels compared to the green pump, facilitating the investigation of the interconnection between different energy levels and population inversion. Moreover, the implementation of high performance red solid-state lasers and advanced plasma sputtering coating technology, known for its high damage threshold, has resulted in the emergence of deep-red lasers operating at the watt level. This study provides additional evidence supporting the enhancement of laser output properties through the excited state absorption (ESA) process, which relies on deep-red and near-infrared excitation.

In this paper, we propose a method for developing a dual-wavelength laser by utilizing the excitation mechanism in Ho^{3+}-doped ZFG fiber. The optimization of the laser cavity was examined, and experiments were conducted. Furthermore, we conducted a comparison between the experimental results and the numerical results. Notably, this technique shows great

promise in enhancing the performance of lasers that utilize other rare-earth ions through the excited state absorption process, paving the way for the advancement of all-fiber ultrafast lasers.

2. THEORETICAL MODEL OF THE Ho^{3+}-DOPED FIBER LASERS

In order to gain a deeper understanding of the doped lasers' excitation and lasing capabilities for achieving optimal performance, we initiated a comprehensive investigation into the spectral characteristics of the gain fiber. As shown in Fig. 1, the emission cross sections of Ho^{3+}:ZFG fiber were examined in both the deep-red and infrared spectral regions through pumping with a homemade 640 nm continuous wave (CW) solid-state laser. The spectral measurements revealed emission cross sections of 1.3×10^{-20} cm^2 for the deep-red wavelength at 750 nm and 0.76×10^{-20} cm^2 for the near-infrared wavelength at 1.2 μm. Significantly, a self-lasing phenomenon at 1.2 μm was observed when the absorbed pump power surpassed 200 mW. Our experimental focus was further directed towards studying the laser generation process using a 640 nm Ho^{3+}:ZFG fiber, with particular attention given to the 750 nm and 1.2 μm fiber laser emissions.

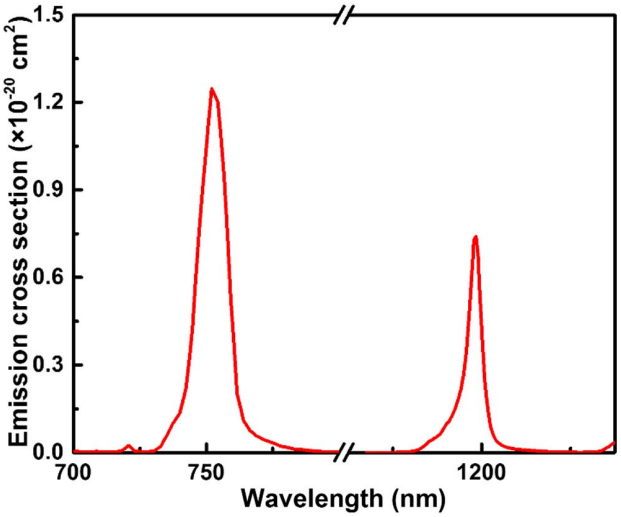

Fig. 1. Emission cross sections of Ho^{3+}:ZFG under 640 nm excitation.

Based on the emission characterization mentioned above, we propose a pumping mechanism for the Ho^{3+} ions in the ZFG fiber, as illustrated in Fig. 2. By absorbing the initial 640 nm photons, the thermalized $^5F_5$ levels are populated from the ground state $^5I_8$ and then non-radiatively decay down to the lower level $^5I_6$. By accumulating the population at $^5I_6$, we can readily achieve the laser emission at 1.2 μm. However, the 640 nm pump wavelength induces excited state absorption from $^5I_6$ to $^5I_5$, resulting in a decrease in laser inversion. This occurs because the pump wavelength at 640 nm is located at the peak of the excited state absorption of the upper level of 1.2 μm. Sequential two-photon absorption further excites the ions to a higher level, which subsequently non-radiatively decay to the metastable levels of $^5F_4$ and $^5S_2$. Nevertheless, the $^5I_7$ level does not have a natural advantage as a lower laser level due to its inherently long lifetime [26]. The significant pump induced excited state absorption from $^5I_7$ limits the population buildup and effectively reduces the effective lifetime of $^5I_7$, which is primarily responsible for the population of $^5I_7$.

3. EXPERIMENTAL RESULTS AND NUMERICAL ANALYSIS

A. All-Fiber Visible and Near-Infrared Ho^{3+}-Doped Lasers

To validate the proposed model, we conducted additional experimental studies. Figure 3(a) illustrates the experimental

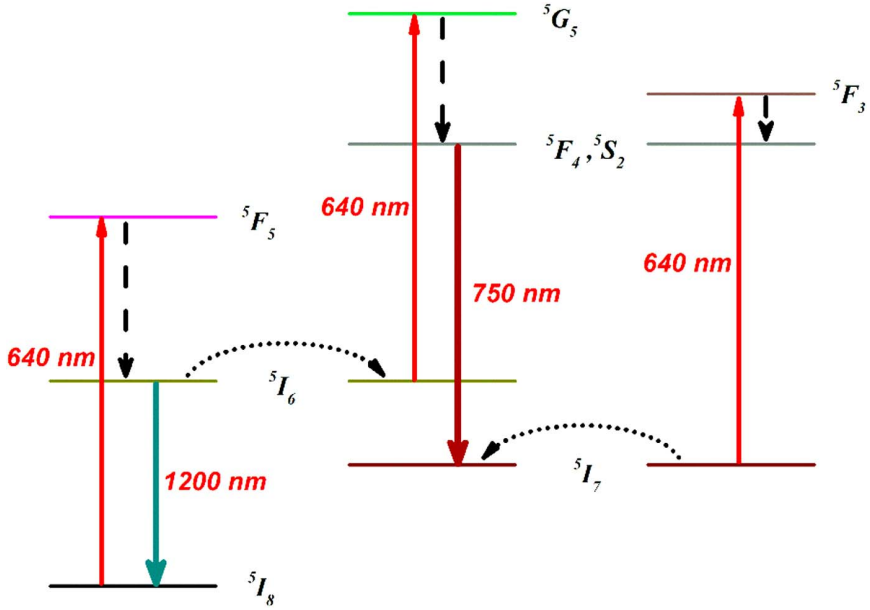

Fig. 2. Proposed two-photon absorption model in Ho^{3+} ions based on the 640 nm pumping process.

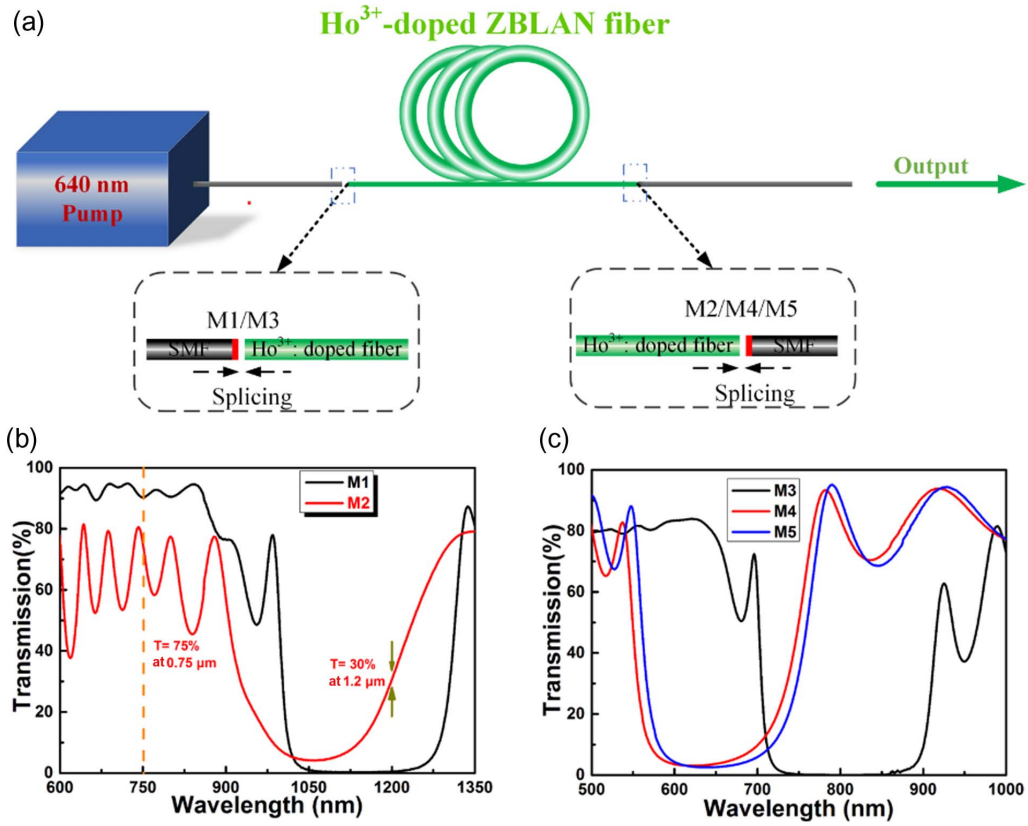

Fig. 3. (a) Experimental setup of Ho^{3+}-doped ZFG all-fiber lasers. Optical transmission properties of the fiber end-facet mirrors: (b) 1.2 μm and (c) 750 nm.

setup of an all-fiber Ho^{3+}-doped fiber laser. The oscillator consists of a pump laser and a gain fiber spliced with single cladding fibers (SCFs) on both ends. The pump laser is a homemade Pr^{3+}:YLF solid-state laser operating at 640 nm, which can provide approximately 1.0 W SCF coupled output power. The gain fiber is a Ho^{3+}:ZFG fiber (from Le Verre Fluoré) with a doping concentration of 5000 ppm (parts per million) Ho^{3+} ions. The fiber has a 7.5/125 μm core/cladding with a 0.24 NA. To enhance the lasing effect, the SCF facets of the Ho^{3+}:ZFG splicing interface are coated with the dielectric. These coatings are fabricated by a remote plasma sputtering system. Figures 3(b) and 3(c) give the optical transmission properties of the fiber end-facet mirrors that we used in this experiment.

To investigate lasing at 1.2 μm using 640 nm pumping, the input mirror (M1) was designed to attain a high transmission of ~94.2% at 640 nm and a high reflectivity of ~99.5% at 1.2 μm. In contrast, the output mirror M2 was designed to exhibit a transmission of ~30% at ~1.2 μm and a low transmission of ~20% at 640 nm to absorb more pump energy in the gain fiber. Four different lengths of Ho^{3+}-doped ZFG fibers (i.e., 20, 30, 40, and 50 cm) were used to investigate the lasing performance at 1.2 μm, and the obtained output characteristics are shown in Fig. 4. The output power of the laser was monitored using a thermopile detector (Coherent, LPM-PM2) equipped with two different dichroic mirrors to isolate the 750 nm and 1.2 μm power levels. The laser thresholds of four different lengths of the gain fibers at 1.2 μm are 37, 69, 73, and 97 mW, respectively. We can see that despite that the output mirror M2 has about 75% transmission around 750 nm, for the gain fiber with a length of 20 cm, dual wavelength lasing appears to emerge as the pump light is increased to ~530 mW. As the length of the gain fiber increased to 30 and 40 cm, the emission threshold for the 750 nm laser also increased, measuring 599 and 653 mW, respectively. The total laser efficiency ($\eta_{\text{total}} = \eta_{1.2\,\mu\text{m}} + \eta_{0.75\,\mu\text{m}}$) gradually increases with the fiber length. It was observed that the slope efficiency of the 1.2 μm emission decreased after surpassing threshold for 750 nm emission. The threshold for the 750 nm emission decreased as the fiber length was shortened, while the corresponding output increased. Moreover, for an active fiber length of 50 cm, a maximum output power of 142 mW was achieved at an absorbed pump power of 900 mW. The corresponding slope efficiency and threshold power are recorded as 16.1% and 120 mW, respectively. It is worth noting that in this case, there is only 1.2 μm single wavelength excitation. Furthermore, this is the first 1.2 μm all-fiber laser generated utilizing a 640 nm laser as the pump.

Figure 5 shows the output spectra of lasing wavelengths around 1.2 μm for the different lengths of the gain fiber starting from 20 to 50 cm with a 10 cm change and their corresponding lasing wavelengths were recorded (optical spectrum analyzer, AQ6315B, Ando) as 1195.76, 1197.50, 1198.40, and 1199.18 nm, respectively. The full width at half maximum (FWHM) of the spectrum varied from 1.6 to 1.1 nm

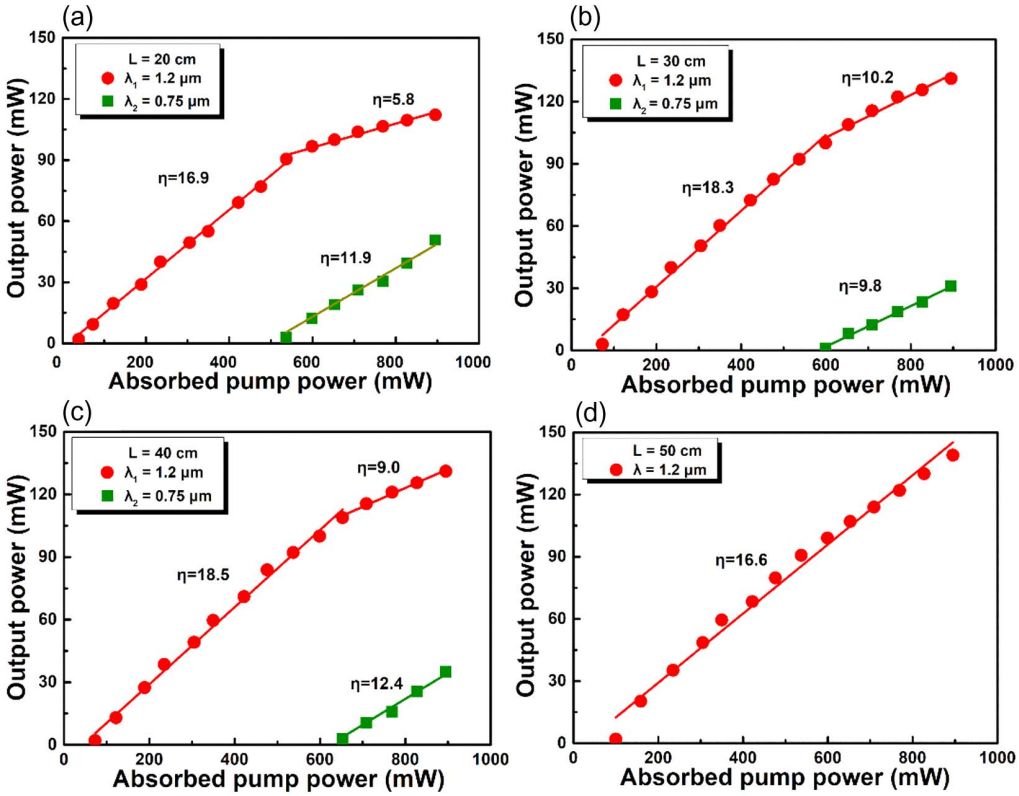

Fig. 4. Measured output power with respect to the absorbed pump powers for active fiber lengths of (a) 20 cm, (b) 30 cm, (c) 40 cm, and (d) 50 cm. The red dots and green squares, respectively, refer to 1.2 μm and 750 nm emissions.

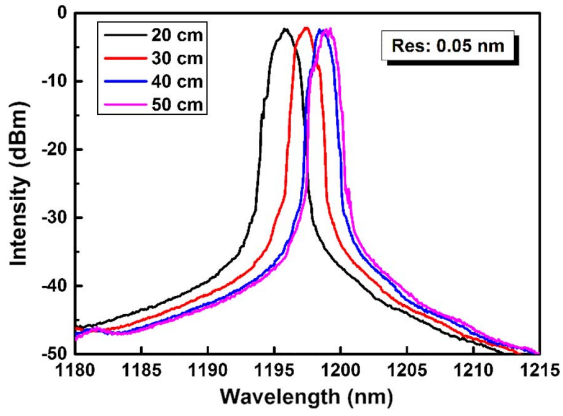

Fig. 5. Near-infrared wavelength based on different lengths of Ho^{3+}:ZFG fiber.

depending on the length of the gain fiber. These results showed that the wavelength of the laser was red shifted as the gain fiber length increased. The variation in the laser output wavelength can be attributed to the influence of sub-levels splitting in the lower energy level and the excited state absorption of pump light in the upper energy level.

Given the successful excitation of the deep-red laser with the high transmission output mirror M2, further investigation was conducted on the deep-red laser, resulting in the development of an all-fiber 640 nm pumped Ho^{3+}:ZFG fiber laser at 750 nm. Figure 6 represents the output characteristics of the all-fiber deep-red fiber lasers. Three different lengths of Ho^{3+}:ZFG fibers (i.e., 13, 20, and 30 cm) were utilized, along with two output mirrors (i.e., M4, M5) with transmission levels of ~50% and ~35% at 750 nm, respectively. The experimental setup employed for this study was identical to the setup in Fig. 3. It can be seen that at a lower pump power scale of less than 1 W, we achieved a maximum power of 271 mW with a slope efficiency of 45.1%, and the lasing threshold was measured as 168 mW. Due to the variance in the pump light absorption capacity of different length gain fibers, for a 20 cm active fiber length, the output power and slope efficiency are greatly enhanced as the output mirror decreases the transmission of the deep-red laser.

B. High Performance Deep-Red Fiber Lasers

Based on these initial results, an optimized laser cavity was designed to maximize the laser output performance for the 750 nm transition. For this purpose, the deep-red laser cavity was constructed by a ~4% Fresnel reflection and ~99.9% high reflection fiber end-facet mirror. As shown in Fig. 7(a), we measured a maximum output power of 1.40 W at a pump power of 3.54 W and the lasing threshold of 0.63 W for an active fiber length of 35 cm. The slope efficiency was estimated to 50.2% at an absorbed pump power of ~3.54 W. For an active fiber length of 20 cm, a maximum output power of 1.34 W was measured for an absorbed pump power of 3.54 W. The slope

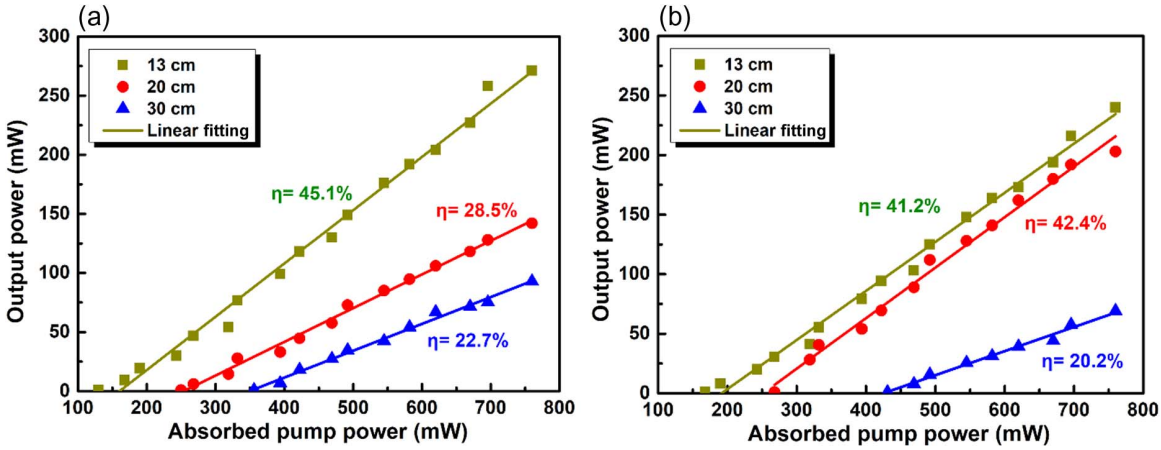

Fig. 6. Output characteristics of all-fiber deep-red Ho^{3+}:ZFG laser with the different output mirrors: (a) M4 and (b) M5.

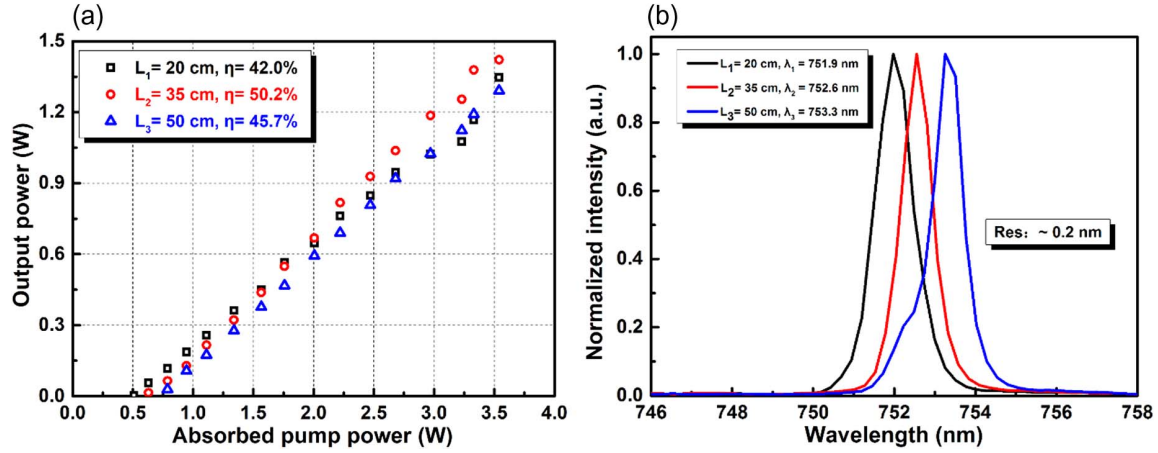

Fig. 7. High output characteristics of Ho^{3+}-doped deep-red fiber laser.

efficiency and threshold were 42.0% and 0.51 W, respectively. At 50 cm active fiber length, the maximum output was 1.29 W for a 3.54 W pump power, the lasing threshold was measured as 0.79 W, and the slope efficiency was 45.7 %. Typical lasing spectra at 751.9, 752.6, and 753.3 nm are corresponding to active fiber lengths of 20, 35, and 50 cm, respectively. As the active fiber length increases, the lasing peak wavelength moves towards the longer wavelength side of the spectrum.

C. Numerical Analysis

We have developed a theoretical model to further investigate the relationship among fiber length, the output mirror reflectivity, and output characteristics. The results are presented in Fig. 8. To streamline the energy level model, the continuous steady-state rate equations of the fiber laser can be stated as [27]

$$\frac{N_2(z)}{N}=\frac{\frac{\Gamma_p\sigma_{ap}[P_p^+(z)+P_p^-(z)]\lambda_p}{hcA}+\frac{\Gamma_s\sigma_{as}[P_s^+(z)+P_s^-(z)]\lambda_s}{hcA}}{\frac{\Gamma_p(\sigma_{ap}+\sigma_{ep})[P_p^+(z)+P_p^-(z)]\lambda_p}{hcA}+\frac{1}{\tau}+\frac{\Gamma_s(\sigma_{as}+\sigma_{es})[P_s^+(z)+P_s^-(z)]\lambda_s}{hcA}}, \tag{1}$$

$$\pm\frac{dP_p^{\pm}(z)}{dz}=-\Gamma_p[\sigma_{ap}N-(\sigma_{ap}+\sigma_{ep})N_2(z)]P_p^{\pm}(z)-\alpha_pP_p^{\pm}(z), \tag{2}$$

$$\pm\frac{dP_s^{\pm}(z)}{dz}=\Gamma_s[(\sigma_{es}+\sigma_{as})N_2(z)-\sigma_{as}N]P_s^{\pm}(z)-\alpha_sP_s^{\pm}(z), \tag{3}$$

where N is the doped ion concentration, N_2 is the laser upper energy level ion concentration, and σ_{ap} and σ_{ep} are the pump absorption and emission cross sections. Similarly, σ_{as} and σ_{es} represent the laser absorption and emission cross sections, λ_p and λ_s are the wavelengths of the pump and laser signal, while α_p and α_s indicate the pump and signal scattering losses, respectively. A is the cross-sectional area of the fiber core, and h is the Planck constant. c is the speed of light in vacuum, and the spontaneous emission lifetime is denoted by τ. The core pump filling factor Γ_p is specified as A_{core}/A_{clad}, while the core laser signal filling factor Γ_s is expressed as [28]

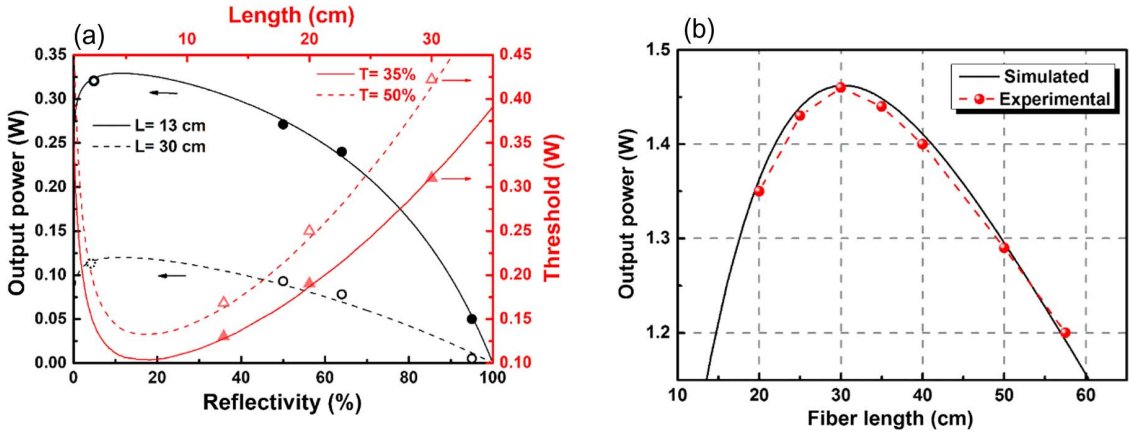

Fig. 8. Experimental and simulated deep-red laser performances at 750 nm. (a) Output power and threshold versus the fiber length and output mirrors' reflectivity; (b) high output power as a function of different fiber lengths.

Table 1. Basic Parameters of Ho^{3+}:ZFG Fiber Lasers Used in the Simulations

Parameter	Value	Parameter	Value
λ_p	640 nm	N	2.935×10^{19} cm^{-3}
λ_s	750 nm	α_p	0.002 cm^{-1}
τ	260 μs	α_s	0.001 cm^{-1}
σ_{ap}	0.39×10^{-20} cm^2	Γ_p	0.0036
σ_{ep}	0.25×10^{-20} cm^2	Γ_s	0.8
σ_{as}	0.20×10^{-20} cm^2	$R_1(\lambda_s)$	0.99
σ_{es}	1.13×10^{-20} cm^2	$R_1(\lambda_p)$	0.15
$R_2(\lambda_s)$	Variable	$R_2(\lambda_p)$	Variable

$$\Gamma(\lambda_s) \approx \frac{\Sigma_\eta |\mu_\eta(\lambda_s)|^2 \Gamma_\eta(\lambda_s) I_\eta g_\eta}{\Sigma_\eta |\mu_\eta(\lambda_s)|^2 I_\eta g_\eta}, \tag{4}$$

where $\Gamma_\eta(\lambda_s)$ represents the mode-field power filling factor, and $\mu_\eta(\lambda_s)$ represents the mode-field coefficient according to the transverse mode in the whole field; g_η denotes the mode-field degradation factor, while I_η denotes the normalized mode. The specific values of the parameters are calculated and summarized in Table 1. Furthermore, in the case of an end-surface pumped high power fiber laser, the boundary conditions are as follows:

$$P_s^+(0) = R_1(\lambda_s) P_s^-(0), \tag{5}$$

$$P_s^-(L) = R_2(\lambda_s) P_s^+(L), \tag{6}$$

$$P_p^+(0) = R_1(\lambda_p) P_p^-(0) + P_{p0}, \tag{7}$$

$$P_p^-(L) = R_2(\lambda_p) P_p^+(L) + P_{pL}, \tag{8}$$

where the positive and negative superscripts in the equations represent the pump or signal light propagation direction in the fiber, and R_1 and R_2 indicate the reflectivity of the input and output mirrors. In addition, $P_p(0)$ and $P_p(L)$ denote the coupled pump power into the front and back ends of the fiber, respectively. The rate equations above are solved using the fourth-order Runge–Kutta method, and the laser output power is simulated by the excellent initial guess function for a simple shooting method [29].

Figure 8(a) shows the deep-red laser output power and the lasing threshold as a function of the output mirror reflectivity and the active fiber length at 750 nm. The solid black and dashed black curves represent the simulated output power characteristics of the gain fiber length of 13 and 30 cm as a function of the output mirror reflectivity using Eq. (3). The solid red and dashed red curves are the simulated threshold powers as a function of fiber length at different output mirror transmissions, i.e., ∼35% and ∼50%, respectively. The circles and the triangles are the experimentally measured data points. These are well fitted on the simulated curves, which tells us the good agreement between the experimental and simulated results. To a certain extent, as the transmission of the output mirror increases, so does the laser output power, until it reaches the Fresnel reflection of the fiber's end face.

We kept the mirror reflection at Fresnel reflection and explored the optimum gain fiber length to obtain maximum output power at 750 nm, and the results are shown in Fig. 8(b). The solid black curve represents the simulated result of the output power as a function of the fiber length where other parameters such as pump power and reflectivity are fixed. For relatively shorter fiber lengths, the laser output power is enhanced substantially as the fiber length increases. As the length increases further, the output power hits its maximum at 30 cm, then falls back, and continues to decrease, which indicates that the background loss in the fiber significantly restricts the laser output power [30]. We also experimentally measured the output powers at different gain fiber lengths varying from 20 to 57.5 cm, which are shown in solid red circles. The dotted red curve is a fitting to experimental data points. The maximum output power at 30 cm is measured as 1.46 W. Simulation and experimental results are in good agreement.

Combined with the above experimental and simulation results, the functioning of the pumping mechanism presented in Fig. 2 was further analyzed. At relatively lower pumping rates, one can easily obtain the lasing at 1.2 μm by pumping at 640 nm, as shown in the energy level diagram. As the pump energies were increased, a population inversion occurred from

levels $^5F_4$, $^5S_2$ to level $^5I_7$. This was experimentally confirmed with the emission of the 750 nm laser at relatively higher threshold pump powers as shown in Fig. 4. Interestingly, despite the strong signal intensity in the deep-red band, excited state absorption from $^5I_7$ to $^5F_3$ becomes more prominent, enabling optimal conversion efficiency of the pump energy into a deep-red laser at 750 nm. The phenomenon is experimentally confirmed with the formation of the cavity at 750 nm with Fresnel reflectivity as shown in Fig. 7(a).

4. CONCLUSION

In summary, we successfully demonstrated the generation of near-infrared lasers at a low pumping rate of 640 nm. Through precise optimization of the laser cavity design, we attained the highest output power noted in single cladding fibers for the deep-red band of an all-fiber laser system. We realized an output power of 271 mW at 750 nm using a Ho^{3+}-doped gain fiber in an all-fiber laser configuration. This is the highest output power achieved in an all-fiber deep-red laser to date. Impressively, the slope efficiency of the all-fiber deep-red laser reached remarkable 45.1%, surpassing the previous records by a factor of ten. Furthermore, our investigation focused on the energy level distribution and spectral properties of Ho^{3+} ions. We postulated and subsequently verified the lasing mechanism via excited level absorption in Ho^{3+}-doped fibers. Employing this mechanism, we developed a deep-red fiber laser with superior output characteristics. This advancement serves as a reference for other rare-earth-doped fiber lasers in the study of excited state absorption, effectively addressing the issue of low output characteristics caused by the long lifetime of lower energy levels in lasing transitions.

Funding. National Natural Science Foundation of China (61975168).

Disclosures. The authors declare no conflicts of interest.

Data Availability. Data underlying the results presented in this paper are not publicly available at this time but may be obtained from the authors upon reasonable request.

REFERENCES

1. M. N. Zervas and C. A. Codemard, "High power fiber lasers: a review," IEEE J. Sel. Top. Quantum Electron. **20**, 219–241 (2014).
2. C. Jauregui, J. Limpert, and A. Tünnermann, "High-power fibre lasers," Nat. Photonics **7**, 861–867 (2013).
3. W. Shi, Q. Fang, X. Zhu, R. A. Norwood, and N. Peyghambarian, "Fiber lasers and their applications," Appl. Opt. **53**, 6554–6568 (2014).
4. A. S. Gomes, A. L. Moura, C. B. de Araújo, and E. P. Raposo, "Recent advances and applications of random lasers and random fiber lasers," Prog. Quantum Electron. **78**, 100343 (2021).
5. H. Wu, R. Li, H. Xiao, L. Huang, H. Yang, J. Leng, and P. Zhou, "First demonstration of a bidirectional tandem-pumped high-brightness 8 kW level confined-doped fiber amplifier," J. Lightwave Technol. **40**, 5673–5681 (2022).
6. W. Yu, P. Yan, T. Qi, Y. Wu, D. Li, Q. Xiao, and M. Gong, "High-power and high-brightness Er:Yb codoped fiber MOPA operating at 1535 nm," Opt. Express **30**, 16837–16846 (2022).
7. B. Anderson, J. Solomon, and A. Flores, "1.1 kW, beam-combinable thulium doped all-fiber amplifier," Proc. SPIE **11665**, 116650B (2021).
8. X. Jin, X. Wang, P. Zhou, H. Xiao, and Z. Liu, "Powerful 2 μm silica fiber sources: a review of recent progress and prospects," J. Electron. Sci. Technol. **13**, 315–327 (2015).
9. B. Beaumont, P. Bourdon, A. Barnini, L. Kervella, T. Robin, and J. L. Gouët, "High efficiency holmium-doped triple-clad fiber laser at 2120 nm," J. Lightwave Technol. **40**, 6480–6485 (2022).
10. S. Ji, S. Liu, X. Lin, Y. Song, B. Xiao, Q. Feng, W. Li, H. Xu, and Z. Cai, "Watt-level visible continuous-wave upconversion fiber lasers toward the "green gap" wavelengths of 535–553 nm," ACS Photonics **8**, 2311–2319 (2021).
11. J. Zou, T. Li, Y. Dou, J. Li, N. Chen, Y. Bu, and Z. Luo, "Direct generation of watt-level yellow Dy^{3+}-doped fiber laser," Photonics Res. **9**, 446–451 (2021).
12. Y. Fujimoto, J. Nakanishi, T. Yamada, O. Ishii, and M. Yamazaki, "Visible fiber lasers excited by GaN laser diodes," Prog. Quantum Electron. **37**, 185–214 (2013).
13. S. Ji, Y. Song, Z. Wang, C. Shen, J. Lin, B. Xiao, Q. Feng, Q. Du, H. Xu, and Z. Cai, "High power downconversion deep-red emission from Ho^{3+}-doped fiber lasers," Nanophotonics **11**, 1603–1609 (2022).
14. W. Li, J. Wu, X. Guan, Z. Zhou, H. Xu, Z. Luo, and Z. Cai, "Efficient continuous-wave and short-pulse Ho^{3+}-doped fluorozirconate glass all-fiber lasers operating in the visible spectral range," Nanoscale **10**, 5272–5279 (2018).
15. S. Ji, X. Lin, M. Chen, X. Rong, H. Xu, W. Li, and Z. Cai, "Green wavelength-tunable and high power Ho^{3+}-doped upconversion fiber lasers," IEEE Photonics Technol. Lett. **32**, 313–316 (2020).
16. X. Zhu and R. Jain, "10-W-level diode-pumped compact 2.78 μm ZBLAN fiber laser," Opt. Lett. **32**, 26–28 (2007).
17. T. Chen, J. Li, J. Yuan, X. Zhou, Y. Ding, L. Wang, J. Zou, Q. Li, Q. Ruan, H. Wang, J. Hong, Y. Bu, and Z. Luo, "3 μm watt-level all-fiber lasers based on mid-IR dielectric-coated fiber mirrors," J. Lightwave Technol. **41**, 249–254 (2023).
18. J. Zou, C. Dong, H. Wang, T. Du, and Z. Luo, "Towards visible-wavelength passively mode-locked lasers in all-fibre format," Light Sci. Appl. **9**, 61 (2020).
19. S. Luo, H. Gu, X. Tang, X. Geng, L. Li, and Z. Cai, "High-power yellow DSR pulses generated from a mode-locked Dy:ZBLAN fiber laser," Opt. Lett. **47**, 1157–1160 (2022).
20. S. Luo, X. Tang, X. Geng, H. Gu, L. Li, and Z. Cai, "Ultrafast true-green Ho:ZBLAN fiber laser inspired by the TD3 AI algorithm," Opt. Lett. **47**, 5881–5884 (2022).
21. Q. Ruan, X. Xiao, J. Zou, H. Wang, S. Fan, T. Li, J. Li, Z. Dong, Z. Cai, and Z. Luo, "Visible-wavelength spatiotemporal mode-locked fiber laser delivering 9 ps, 4 nJ pulses at 635 nm," Laser Photonics Rev. **16**, 2100678 (2022).
22. S. Ji, S. Huang, Z. Wang, X. Lin, B. Xiao, H. Xu, and Z. Cai, "Watt-level high-efficiency deep-red Ho^{3+}:ZBLAN fiber laser," J. Lightwave Technol. **41**, 301–306 (2023).
23. S. Ji, Z. Wang, S. Huang, C. Shen, J. Lin, B. Xiao, Q. Feng, H. Xu, and Z. Cai, "532 nm pumped visible emission from Ho^{3+}-doped fiber lasers," Opt. Laser Technol. **158**, 108900 (2023).
24. X. Zhu, J. Zong, K. Wiersma, R. A. Norwood, N. S. Prasad, M. D. Obland, A. Chavez-Pirson, and N. Peyghambarian, "Watt-level short-length holmium-doped ZBLAN fiber lasers at 1.2 μm," Opt. Lett. **39**, 1533–1536 (2014).
25. Y. Ma, X. Zhu, L. Yang, X. Zhang, R. A. Norwood, and N. Peyghambarian, "Wavelength tunable Ho^{3+}-doped ZBLAN fiber lasers in the 1.2 μm wavelength region," IEEE Photonics Technol. Lett. **30**, 1483–1486 (2018).
26. M. Chen, W. Li, S. Ji, X. Lin, X. Zhan, H. Xu, and Z. Cai, "Study on fluorescence characteristics of the Ho^{3+}:ZBLAN fiber under ~640 nm excitation," Opt. Mater. **97**, 109351 (2019).
27. I. Kelson and A. A. Hardy, "Strongly pumped fiber lasers," IEEE J. Quantum Electron. **34**, 1570–1577 (1998).
28. E. Yahel and A. A. Hardy, "Modeling and optimization of short Er^{3+}-Yb^{3+} codoped fiber lasers," IEEE J. Quantum Electron. **39**, 1444–1451 (2003).
29. X. Hu, T. Ning, L. Pei, Q. Chen, and J. Li, "Excellent initial guess functions for simple shooting method in Yb^{3+}-doped fiber lasers," Opt. Fiber Technol. **20**, 358–364 (2014).
30. W. Wang, L. Li, D. Chen, and Q. Zhang, "Numerical analysis of 2.7 μm lasing in Er^{3+}-doped tellurite fiber lasers," Sci. Rep. **6**, 31761 (2016).